Author Manuscript

Author Manuscript

Author Manuscript

Author Manuscript

HHS Public Access

Author manuscript

Magn Reson Med. Author manuscript; available in PMC 2018 February 12.

Published in final edited form as:

Magn Reson Med. 2017 November ; 78(5): 2048–2054. doi:10.1002/mrm.26562.

Sensitive Enhancement of Vessel Wall Imaging With an Endoesophageal Wireless Amplified NMR Detector (WAND)

Xianchun Zeng[1,3], **Mladen Barbic**[2], **Liangliang Chen**[3], and **Chunqi Qian**[3,*]

[1]Department of Radiology, Guizhou Provincial People's Hospital, Guiyang, China

[2]Applied Physics and Instrumentation Group, Howard Huge Medical Institute, Janelia Research Campus, Ashburn, Virginia, USA

[3]Department of Radiology, Michigan State University, East Lansing, Michigan, USA

Abstract

Purpose—To improve the imaging quality of vessel walls with an endoesophageal Wireless Amplified NMR Detector (WAND).

Methods—A cylindrically shaped double-frequency resonator has been constructed with a single metal wire that is self-connected by a pair of nonlinear capacitors. The double-frequency resonator can convert wirelessly provided pumping power into amplified MR signals. This compact design makes the detector easily insertable into a rodent esophagus.

Results—The detector has good longitudinal and axial symmetry. Compared to an external surface coil, the WAND can enhance detection sensitivity by at least 5 times, even when the distance separation between the region of interest and the detector's cylindrical surface is twice the detector's own radius. Such detection capability enables us to observe vessel walls near the aortic arch and carotid bifurcation with elevated sensitivity.

Conclusion—A cylindrical MRI detector integrated with a wireless-powered amplifier has been developed as an endoesophageal detector to enhance detection sensitivity of vessel walls. This detector can greatly improve the imaging quality for vessel regions that are susceptible to atherosclerotic lesions.

Keywords

wireless amplifier; cylindrical endoesophageal detector

INTRODUCTION

It is well known in the MR community that a smaller detector has higher local sensitivity when it is placed in vicinity to the region of interest (ROI) (1,2). It is also a common practice to connect the detector with a transistor-based, low-noise amplifier in order to minimize

*Correspondence to: Chunqi Qian, Department of Radiology, Michigan State University, 846 Service Road, East Lansing, MI 48824, USA. qianchu1@msu.edu; Twitter: @qianchq.

SUPPORTING INFORMATION

Additional supporting information can be found in the online version of this article.

Author Manuscript Author Manuscript Author Manuscript Author Manuscript

sensitivity loss during subsequent stages signal transmission (3). This method of amplification is effective only if a hard-wired connection can be used. When the smaller detector is used inside the body as an implantable or interventional device, however, a hardwired connection is often inconvenient or impractical, attributed to increased risk of infection and radiofrequency (RF) heating. Whereas MR signals can be wirelessly transmitted by mutual inductive coupling between the internal detector and the external receiver (4), the coupling efficiency may be small, especially when the internal detector is deep inside the body. Recently, it has been demonstrated that the efficiency of wireless signal transmission can be greatly improved by a wirelessly powered amplifier that is integrated with the detection coil (5,6) based on the principle of parametric amplification (7–9). This Wireless Amplified NMR Detector (WAND) was surgically implanted onto the surface of a rat kidney to observe individual nephrons in vivo (10,11). Here, we want to demonstrate a nonsurgical use of the WAND: A newly designed cylindrical detector with good longitudinal homogeneity and axial symmetry can be easily inserted into the esophagus to observe surrounding vessels. This detector is effective even when the distance separation between the ROI and the detector's cylindrical surface is twice the detector's own radius. Such detection capability makes it possible to image vessel walls (12) of deep lying arteries with improved sensitivity and spatial resolution. This endoesophageal WAND could be used in patients to better characterize vulnerable or ulcerative plaques near the aortic arch or carotid bifurcation. It may also help to precisely identify subtle ruptures of aortic dissection, enabling better treatment for this life-threatening condition.

METHODS

Detector Construction

Wireless-powered amplification relies on nonlinear capacitance to transfer energy from the externally provided pumping field to weak MR signals (5). The detector can be implemented as a nonlinear double-frequency resonator (10), whose lower-resonance mode can receive MR signals at the Larmor frequency, ω_1, and whose higher-resonance mode is sensitive to a pumping field at a frequency, ω_3, that is slightly above $2\omega_1$. The frequency offset between ω_3 and $2\omega_1$ should be at least the imaging bandwidth, so that the "idler signals" created at the difference frequency, $\omega_2=\omega_3-\omega_1$, can be filtered out to eliminate destructive interference with MR signals at ω_1. Previous designs of the WAND used Foster's networks to create multiple resonance modes (13). These designs generated an asymmetric magnetic field pattern by its constituting inductors. Here, a cylindrical detector is constructed with good longitudinal and axial symmetry. As shown in the schematics in Figure 1a, the circuit consists of three leg inductors (L_1, L_3, and L_2) that are serially connected. The gaps between legs and rings are bridged by two identical zero-biased varactors (C_1 and C_2). L_1 and L_2 are symmetrically distributed with respect to L_3 to maintain axial symmetry of the resonator's detection profile. Their span angle, ψ, is empirically adjusted near 90° to make the higher-resonance frequency approximately twice the lower-resonance frequency. The high-frequency mode is sensitive to a pumping field, B_{pump}, perpendicular to the rectangular loop labeled in red, and the low-frequency mode is sensitive to nuclear magnetization precessing in the horizontal plane. The cathode of C_1 is connected to the anode of C_2, so that their capacitances are modulated by the pumping field in the same manner. Figure 1b shows the

Author Manuscript Author Manuscript Author Manuscript Author Manuscript

front and rear views of a 9.2-mm-long WAND. It is made of a 32-gauge copper wire mounted on a 3-mm-diameter polyurethane cylinder. The metal wire is self-connected by two varactors shown in black (BB145B; NXP Semiconductors, Eindhoven, the Netherlands). According to S_{21} measurement, the WAND has resonance frequencies at 302 (Q=62) and 606 MHz (Q=40) in its passive state. When a pumping field is applied to reach a power level of approximately 0.4 dB below the resonator's oscillation threshold, the WAND has more than 20 dB of gain at the Larmor frequency of 300.3 MHz (Fig. 1c). Meanwhile, the amplified resonator also has a reduced bandwidth of ~300 kHz at −3 dB, which is still enough for most MRI experiments.

MRI Experiments

The cylindrical WAND was coated by a thin layer of medical grade epoxy before insertion into the detection object. A four-element surface coil for rat brain (Bruker Biospin) was placed beneath the detection object with about 22-mm distance separation from the WAND. A pair of pumping loops was placed orthogonally to the surface coil (Fig. 2a). The entire assembly (Fig. 2b) was then inserted into a 7 Tesla (T) magnet equipped with a 77-mm bore volume coil and an AVANCE III console (Bruker BioSpin, Billerica, MA). During RF excitation, both varactors were strongly modulated to decouple the WAND from the volume coil. During signal acquisition, the pumping power was turned on and adjusted around 10 mW to approximately 0.4 dB below the resonator's oscillation threshold, so that the signal transmission efficiency between the WAND and the external surface coil was greatly improved.

The performance of the WAND was evaluated on a water phantom. Multislice 2D gradient recalled echo (GRE) images were acquired in a series of detection configurations with the following parameters: repetition time/echo time (TR/TE)=500/3.5 ms; 30° flip angle; 3×3cm^2 field of view (FOV); 0.4-mm slice thickness; 300×300 matrix; and 25-kHz imaging bandwidth. First, only the external surface coil was used. Second, the WAND was inserted into the water phantom and passively coupled to the external surface coil. Third, the WAND actively amplified signals from its surrounding in the presence of pumping power. Finally, B_1 homogeneity near the WAND was measured by the double-angle method (14).

All animal experiments were approved by the Institutional Animal Care and Use Committee at Michigan State University. During in vivo experiments, the WAND was inserted into the esophagus of a ~300-g rat. The rat was anesthetized with isoflurane and secured in the prone position under ventilation. The insertion depth of the WAND was empirically adjusted by an insertion rod until the WAND's sensitive region appears in the axial slice across the aortic arch or carotid bifurcation. Transverse slices were first acquired with flow-compensated GRE sequences to locate major arteries near the esophagus. Longitudinal slices were subsequently acquired with flow-saturated GRE sequences to observe lumen walls in the absence and presence of active amplification. Detailed acquisition parameters are listed in figure captions and summarized in the Supporting Table S1.

Author Manuscript Author Manuscript Author Manuscript Author Manuscript

Data Processing

All images were processed using Matlab (The Mathworks, Inc., Natick, MA, USA). To quantitatively evaluate the effective detection range of the WAND in water phantoms, 2D images acquired with and without active amplification were normalized to the same noise floor. These normalized images were used to obtain relative sensitivity maps by dividing them with the sensitivity-normalized images acquired using only the external surface coil. To demonstrate the sensitivity advantage of the amplified resonator over the passive resonator for in vivo applications, 1D intensity profiles were plotted across lumen walls. Derivative plots for these 1D intensity profiles were also obtained to locate lumen boundaries with abrupt changes in signal intensity (15). Positions of lumen boundaries can be identified with 95% confidence when the absolute values of local derivatives exceed twice the standard deviation (SD) evaluated over the entire derivative plot.

RESULTS

Figure 3 shows the axial (row 1), coronal (row 2), and sagittal (row 3) images acquired with the external surface coil (column 1), with the passive resonator (columns 2 and 3) and with the amplified resonator (column 4). For regions very close to the detector's surface, sensitivity enhancement is clearly demonstrated by the 1D intensity profiles shown in row 4: The passive resonator has approximately 3 times the sensitivity of the external surface coil, and the amplified resonator has approximately 11 times the sensitivity. For regions farther away from the detector, relative sensitivity maps are calculated for the passive and amplified resonators to estimate the resonator's effective detection range. As shown in the axial profile for the passive resonator (column 5), the sensitivity enhancement pattern is orientation dependent, especially for regions to the right side of the resonator. These regions are closer to the resonator's rectangular loop containing the two varactors. This loop is more sensitive to the pumping field, but less sensitive to MR signals. On the other hand, the amplified resonator has larger effective range and better axial symmetry: For the majority of orientations in the axial profile (column 6), sensitivity is enhanced by at least a factor of 5 for distance separations up to 3mm from the detector's surface, when compared to detection by the external surface coil. Such a level of sensitivity enhancement is mostly maintained within a 7-mm region in the longitudinal direction, as shown by the coronal and sagittal profiles in column 6. According to the flip angle maps in column 7, the WAND introduces little disturbance on the flip angle, demonstrating the effectiveness of varactor decoupling during RF excitation. It is noteworthy to mention that the resonator has a gain variation of less than 0.4 dB within the 25-kHz imaging bandwidth. Such a level of gain variation has introduced negligible artifacts in all the amplified images.

Figure 4a is the axial slice acquired across ascending arteries stemming from the aortic arch with the detector inserted inside the esophagus. Figure 4b1 and 4c1 is longitudinal slices acquired along the dashed line defined in Figure 4a with passive coupling and active amplification, respectively. For the image acquired with passive coupling (Fig. 4b1), vessels are visible only near the aortic arch, owing to the stronger B_1 field near the passive resonator (4,16). For the actively amplified image in Figure 4c1, vessel walls and fascia structures are clearly visible near the aorta's junctions with the common carotid artery and the subclavian

Author Manuscript Author Manuscript Author Manuscript Author Manuscript

artery. Based on the intensity profile comparison between the passively coupled and the actively amplified resonator (Supporting Fig. S1), amplification leads to at least 3 times gain in sensitivity over passive coupling. As shown in the derivative plot for the amplified image (Fig. 4c2), there are multiple sharp peaks whose absolute heights exceed twice the SD. These peaks correspond to positions where lumen walls can be identified with 95% confidence. In comparison, the derivative plot for the passive resonator has fewer identifiable peaks (Fig. 4b2), attributed to the lower sensitivity of the passive resonator.

The WAND can enhance the detection sensitivity of aortic arch, whose distance separation from the detector's surface is less than 1.5mm. For regions farther away from the esophagus, the WAND can demonstrate its sensitivity advantage as well. As shown in the axial image in Figure 5a, the longitudinal plane passing through the bifurcated carotid arteries is approximately 3.5mm away from the detector's surface. This distance separation is larger than the detector's own diameter. But compared to Figure 5b1, the actively amplified image in Figure 5c1 provides much better views of smooth vessel walls and clear lumens. The sensitivity advantage of amplified resonator is clearly demonstrated by the 1D intensity profiles in Supporting Figure S2. In the derivative plot for the amplified image (Fig. 5c2), the pair of negative and positive peaks that exceed twice the SD correspond to lumen walls of the common carotid artery. In comparison, the positive peak is missing in Figure 5b2, attributed to the lower sensitivity of the passive resonator.

DISCUSSION

In this work, a cylindrically shaped WAND is fabricated and inserted into the rodent esophagus to observe vessel walls at closer distances. Owing to its enhanced detection sensitivity, vessel walls in the aortic arch and carotid bifurcation can be imaged with greatly improved quality. This endoesophageal detector could be useful to monitor plaque progression in atheroma susceptible transgenic rats. It may also be used to characterize inflammation or carcinogenesis in thyroid and lymph nodes near rodents' esophagus.

This endoesophageal WAND has several favorable features. First, it offers an efficient and convenient way to enhance MR sensitivity. It can utilize the wirelessly provided pumping power to sensitively detect and simultaneously amplify MR signals. Only ~10 mW of pumping power is required on the external pumping loop to drive the WAND at a penetration depth of ~22mm. This level of pumping power is negligible to induce measurable local heating. Because MR signals are transmitted wirelessly, a standard commercial coil can be used externally to pick up these amplified signals, without the need for a specialized hardware interface. Second, the WAND is a cylindrical detector that can be easily inserted into body lumens. It creates a cylindrical detection profile with reasonable axial symmetry. Compared to the external surface coil, it can enhance signal-to-noise ratio (SNR) by a factor of 5 for regions within 3-mm separation from its surface, even though the detector's radius is only half this distance separation. Such detection capability allows the WAND to sensitively observe multiple important vessels from inside the esophagus, without the need for surgical incisions. Third, the WAND is a wireless detector with reduced coupling to the RF excitation field. It has two zero-biased varactors that can be strongly modulated by the excitation pulse. Unlike hard-wired connections that may generate a

Author Manuscript Author Manuscript Author Manuscript Author Manuscript

position-dependent coupling profile attributed to wavelength effect, the WAND's decoupling efficiency is independent of its insertion depth. This favorable feature could make the wireless amplifier an alternative to hard-wired connection for improved RF safety in interventional detectors. Although the parametric amplifier is somewhat noisier than a transistor-based amplifier using hard-wired connections, the WAND is still much more sensitive than the external surface coil by its ability to retain around 72% sensitivity of a directly connected coil of the same dimension. Fourth, the WAND has a very compact design. It consists of only a thin metal wire that is self-connected with two varactor diodes. This compact design makes the WAND amenable to geometric scaling. As a rule of thumb, if the WAND's dimension is uniformly scaled down by a factor of 2, its effective inductance will also be scaled down by a factor of 2, and a pair of varactor diodes with twice the zero-biased capacitance is required to maintain its operating resonance frequency around 300 MHz. Such a simple scaling relation is particularly useful for the design of further miniaturized detectors used inside narrower lumens. These miniaturized detectors can be used inside rats' small intestine to sensitively characterize subepithelial inflammation or tumor infiltration. Conversely, the detector's dimension can also be uniformly scaled up by a factor of 5.5 to increase its length to 50.6mm and its diameter to 16.5mm, in order to fit into the esophagus of large animals or humans. Using the same pair of varactors (BB145B; NXP Semiconductors), the WAND's operating frequency can be tuned down to ~128 Mhz. These enlarged detectors can be used in a clinical 3T scanner to characterize vulnerable plaques or dissected vessels in humans. They may also be used to characterize thyroid lesions with improved accuracy or identify underlying reasons for lymph-node enlargements near the esophagus.

CONCLUSION

An endoesophageal detector integrated with a wirelessly powered amplifier is developed to improve MRI sensitivity of vessel walls. Such a detector could be used to characterize deep-lying lesions near the esophagus. The wireless powered amplifier can also eliminate the need for hard-wired connections normally used in endovascular (17), endorectal (18), or intraoral coils (19,20), thus improve their operation flexibility.

Supplementary Material

Refer to Web version on PubMed Central for supplementary material.

Acknowledgments

Grant sponsor: NIBIB; Grant number: R00EB016753; Grant sponsor: Department of Radiology at Michigan State University.

The authors thank Dr Alan Koretsky and Dr Joe Murphy- Boesch for their inspirations from the initial stage of this project. M.B. acknowledges the Howard Hughes Medical Institute for support. Technical assistance from Ms. Yingsang Wu is also appreciated. The content of this paper does not necessarily represent official views of the NIH.

References

1. Murphyboesch J, Koretsky AP. An In vivo NMR probe circuit for improved sensitivity. J Magn Reson. 1983; 54:526–532.

Author Manuscript Author Manuscript Author Manuscript Author Manuscript

2. Olson DL, Peck TL, Webb AG, Magin RL, Sweedler JV. High-resolution microcoil 1h-nmr for mass-limited, nanoliter-volume samples. Science. 1995; 270:1967–1970.
3. Hoult D. The NMR receiver: a description and analysis of design. Prog Nucl Magn Reson Spectrosc. 1978; 12:41–77.
4. Schnall MD, Barlow C, Subramanian VH, Leigh JS. Wireless implanted magnetic-resonance probes for in vivo NMR. J Magn Reson. 1986; 68:161–167.
5. Qian CQ, Murphy-Boesch J, Dodd S, Koretsky AP. Sensitivity enhancement of remotely coupled NMR detectors using wirelessly powered parametric amplification. Mag Res Med. 2012; 68:989–996.
6. Syms RRA, Solymar L, Young IR. Three-frequency parametric amplification in magneto-inductive ring resonators. Metamaterials. 2008; 2:122–134.
7. Martius, S., Heid, O., Vester, M., Biber, S., Nistler, J. Wireless local coil signal transmission using a parametric upconverter. Proceedings of the 17th Annual Meeting of ISMRM; 2009. p. 2934
8. Cork, P., Hulbert, AP., Hunt, J. Parametric amplifier device. US Patent. 8638102 B8638102. 2010.
9. Reykowski, A. System and method for a mode balanced parametric amplifier. US Patent. 9207297 B9207292. 2015.
10. Qian CQ, Yu X, Chen DY, et al. Wireless Amplified Nuclear MR Detector (WAND) for high-spatial-resolution MR imaging of internal organs: preclinical demonstration in a rodent model. Radiology. 2013; 268:228–236. [PubMed: 23392428]
11. Qian C, Yu X, Pothayee N, Dodd S, Bouraoud N, Star RA, Koretsky AP. Live nephron imaging by MRI. Am J Physiol Renal Physiol. 2014; 307:F1162–F1168. [PubMed: 25186296]
12. Underhill HR, Hatsukami TS, Fayad ZA, Fuster V, Yuan C. MRI of carotid atherosclerosis: clinical implications and future directions. Nat Rev Cardiol. 2010; 7:165–173. [PubMed: 20101259]
13. Foster RM. A reactance theorem. Bell Syst Tech J. 1924; 3:259–267.
14. Cunningham CH, Pauly JM, Nayak KS. Saturated double-angle method for rapid B-1 plus mapping. Magn Reson Med. 2006; 55:1326–1333. [PubMed: 16683260]
15. Canny J. A computational approach to edge-detection. IEEE Trans Pattern Anal Mach Intell. 1986; 8:679–698. [PubMed: 21869365]
16. Burl M, Coutts GA, Young IR. Tuned fiducial markers to identify body locations with minimal perturbation of tissue magnetization. Magn Reson Med. 1996; 36:491–493. [PubMed: 8875424]
17. Atalar E, Bottomley PA, Ocali O, Correia LCL, Kelemen MD, Lima JA, Zerhouni EA. High resolution intravascular MRI and MRS by using a catheter receiver coil. Magn Reson Med. 1996; 36:596–605. [PubMed: 8892213]
18. Schnall MD, Lenkinski RE, Pollack HM, Imai Y, Kressel HY. Prostate: MR imaging with an endorectal surface coil. Radiology. 1989; 172:570–574. [PubMed: 2748842]
19. Li, R., Bishop, P., Jesmanowicz, A., Nencka, A., Stephenson, JB., IV, Pawela, C., Yan, JG., Hudetz, AG., Matloub, H., Hyde, JS. Improving whole brain coverage and Signal-to-Noise ratio using novel intra-oral and over head surface coil array in rat under 9.4T. Proceedings of the 19th Annual Meeting of ISMRM; 2011. p. 1822
20. Idiyatullin D, Corum CA, Nixdorf DR, Garwood M. Intraoral approach for imaging teeth using the transverse B-1 field components of an occlusally oriented loop coil. Magn Reson Med. 2014; 72:160–165. [PubMed: 23900995]

Author Manuscript Author Manuscript Author Manuscript Author Manuscript

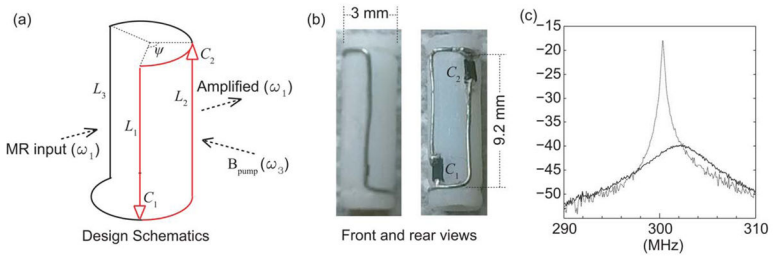

FIG. 1.

The schematic diagram (**a**) and the pictures (**b**) of a cylindrically shaped WAND. The detector is made of a 32-gauge metal wire mounted on a 3-mm-diameter cylinder over a 9.2-mm length. The metal wire is self-connected by two varactor diodes (C_1 and C_2) bridging across the gaps. The two leg inductors (L_1 and L_2) are symmetrically distributed with respect to L_3. The rectangular loop containing the two varactors creates the high-frequency resonance mode, whereas the low-frequency mode generates a magnetic field that is parallel to this rectangular loop. The span angle, ψ, between L_1 and L_2 can be empirically adjusted around 90° to make the higher-resonance frequency approximately twice the lower-resonance frequency. (**c**) S_{21} curve measured with a double pick-up loop placed above the resonator and connected to a network analyzer. The solid curve is measured in the absence of pumping power, and the dotted curve is measured in the presence of pumping power that is approximately 0.4 dB below the resonator's oscillation threshold.

Author Manuscript Author Manuscript Author Manuscript Author Manuscript

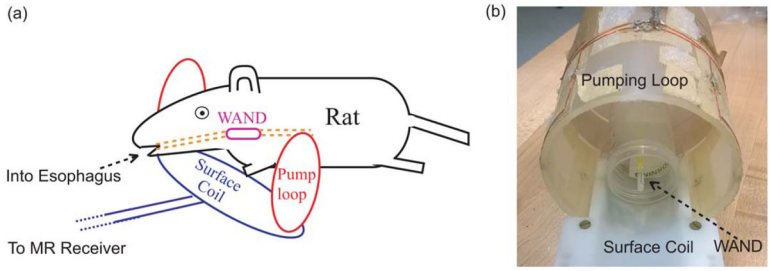

FIG. 2.

(**a**) WAND device inserted inside the rat esophagus that couples inductively to the external surface coil and the pair of pumping loops. The surface coil is placed beneath the rat to receive amplified MR signals, and the pair of pumping loops is placed orthogonally to wirelessly power up the amplifier. (**b**) Phantom test arrangement with the WAND inserted in the center of a water tube placed above the surface coil. The distance separation between the WAND and the external surface coil is approximately 22mm.

Author Manuscript Author Manuscript Author Manuscript Author Manuscript

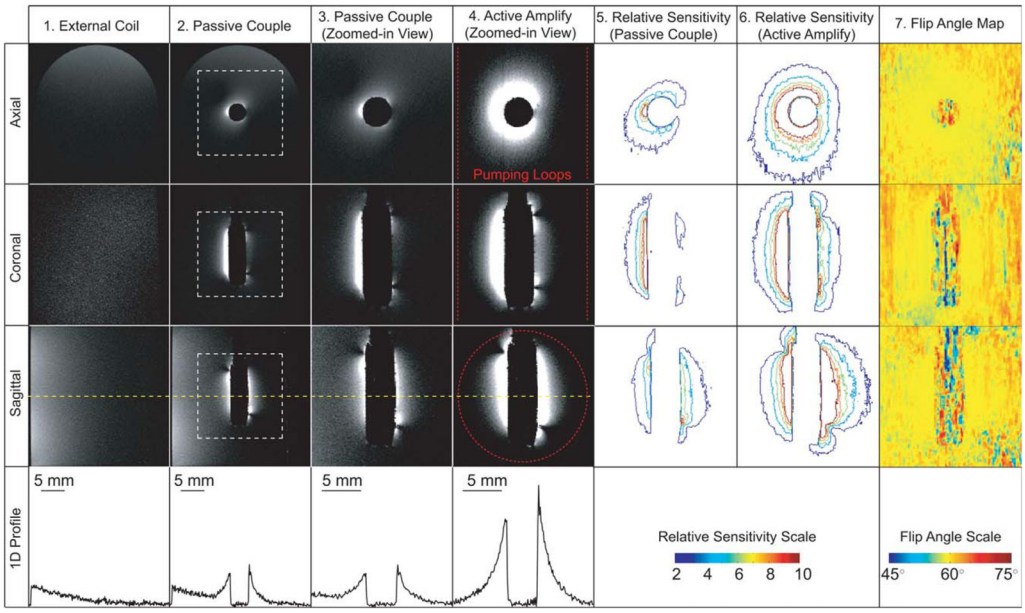

FIG. 3.

2D GRE images of a water phantom acquired in three orientations, using TR/TE=500/3.5 ms, 30° flip angle, 3×3cm^2 FOV, 0.4-mm slice thickness, 300×300 matrix, and 25-kHz imaging bandwidth. Images in column 1 were acquired with the external surface coil only. Images in column 2 were acquired with passive coupling to the resonator. Zoomed-in views of image regions defined by the dashed square are shown in column 3. Column 4 shows zoomed-in views acquired with active amplification, where the pair of pumping loops is schematically represented by red dashed lines. Column 5 shows the relative sensitivity of images acquired by the passive resonator with respect to those images acquired by the external surface coil. Column 6 shows the relative sensitivity of images acquired by the amplified resonator with respect to those images acquired by the external surface coil. Column 7 shows flip angle maps of the amplified resonator obtained using the double-angle method with 60° and 120° excitations (14), with TR=5 seconds and the remaining parameters the same as above. The fourth row shows 1D intensity profiles taken along the dashed lines shown on the sagittal sections in the third row. Their vertical axes are scaled to the same noise level to make their heights a measure of relative sensitivity. CCA, common carotid artery; SubA, subclavian artery.

Author Manuscript Author Manuscript Author Manuscript Author Manuscript

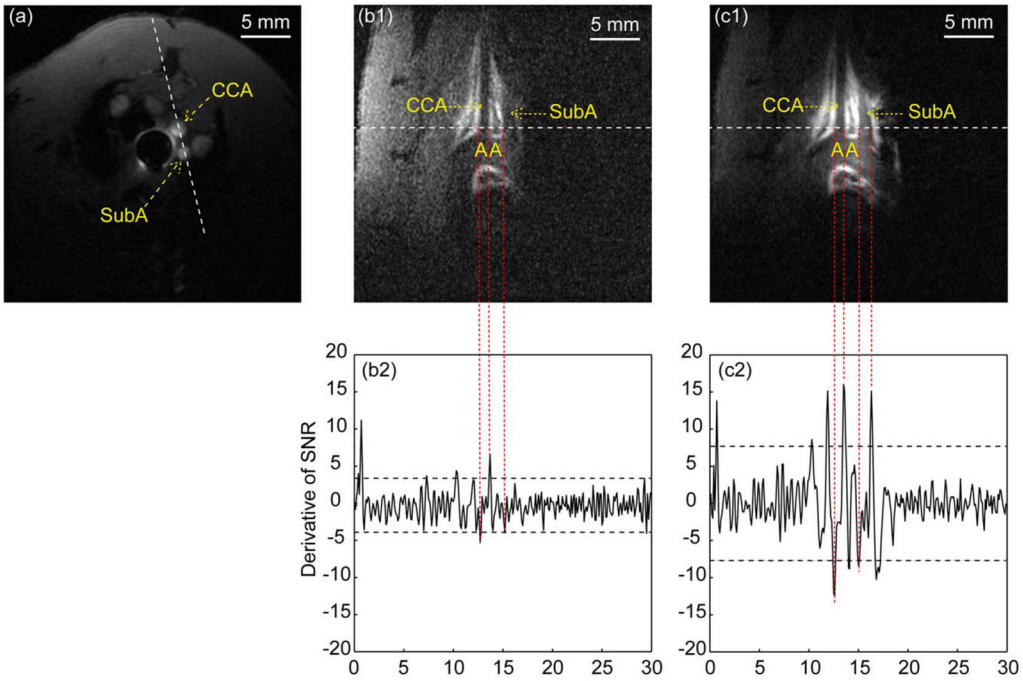

FIG. 4.

(**a**) Axial slice to locate ascending arteries stemming from the aortic arch when the passive resonator is inserted inside the esophagus. The acquisition parameters are TR/TE=111/2.5 ms, 35° flip angle, 3×3cm^2 FOV, 0.8mm slice thickness, 256×256 matrix, and number of acquisitions (NA)=4. The dashed line passing through the common carotid artery and subclavian artery defines the orientation of longitudinal images to be acquired subsequently. (**b1**) Longitudinal slice acquired with flow saturation in the absence of pumping power. The acquisition parameters are TR/TE=79/3.5 ms, 17° flip angle, 3×3cm^2 FOV, 0.4-mm slice thickness, 300×300 matrix, and NA=8. (**c1**) Longitudinal slice acquired in the presence of pumping power, with other acquisitions parameters the same as (**b1**). Bandwidths for all three images are 25 kHz. (**b2**) and (**c2**) are derivative plots of 1D intensity profiles normalized to the same noise floor when plotted along the dashed lines in (**b1**) and (**c1**). Horizontal dashed lines in (**b2**) and (**c2**) correspond to twice the SD evaluated over each derivative plot. CCA, common carotid artery; SubA, subclavian artery.

Author Manuscript Author Manuscript Author Manuscript Author Manuscript

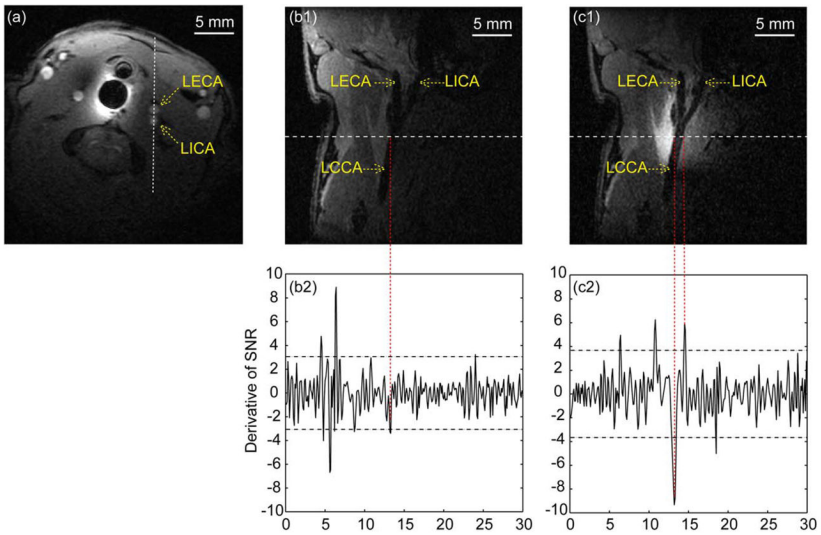

FIG. 5.

(**a**) Axial slice to locate carotid bifurcation when the passive resonator is inserted inside the esophagus. The acquisition parameters are TR/TE=163.3/2.5 ms, 35° flip angle, 3×3cm^2 FOV, 0.8-mm slice thickness, 256×256 matrix, and number of acquisitions (NA)=2. The dashed line passing through the internal and external carotid arteries defines the orientation of longitudinal images to be acquired subsequently. (**b1**) Longitudinal slice acquired with flow saturation in the absence of pumping power. The acquisition parameters are TR/TE=348.5/4.3 ms, 32° flip angle, 3×3cm^2 FOV, 0.4-mm slice thickness, 300×300 matrix, and NA=4. (**c1**) Longitudinal slice acquired in the presence of pumping power, with other acquisition parameters the same as (**b1**). The bandwidths for all three images are 25 kHz. (**b2**) and (**c2**) are derivative plots of 1D intensity profiles normalized to the same noise floor when plotted along the dashed lines in (**b1**) and (**c1**) and the horizontal dashed lines correspond to twice the SD evaluated over each derivative plot. LECA, left external carotid artery; LICA, left internal carotid artery; LCCA, left common carotid artery.